

A Jacobian-free Multigrid Preconditioner for Discontinuous Galerkin Methods applied to Numerical Weather Prediction

Philipp Birken¹, Andreas Dedner², Robert Klöfkor^{1*}

¹Center for Mathematical Sciences, Lund University, Box 117, Lund, 22100, Sweden.

²Mathematics Institute, University of Warwick, Coventry, CV4 7AL, UK.

*Corresponding author(s). E-mail(s): robertk@math.lu.se;

Contributing authors: philipp.birken@math.lu.se;

A.S.Dedner@warwick.ac.uk;

Abstract

Discontinuous Galerkin (DG) methods are promising high order discretizations for unsteady compressible flows. Here, we focus on Numerical Weather Prediction (NWP). These flows are characterized by a fine resolution in z -direction and low Mach numbers, making the system stiff. Thus, implicit time integration is required and for this a fast, highly parallel, low-memory iterative solver for the resulting algebraic systems. As a basic framework, we use inexact Jacobian-Free Newton-GMRES with a preconditioner.

For low order finite volume discretizations, multigrid methods have been successfully applied to steady and unsteady fluid flows. However, for high order DG methods, such solvers are currently lacking. This motivates our research to construct a Jacobian-free preconditioner for high order DG discretizations. The preconditioner is based on a multigrid method constructed for a low order finite volume discretization defined on a subgrid of the DG mesh. We design a computationally efficient and mass conservative mapping between the grids. As smoothers, explicit Runge-Kutta pseudo time iterations are used, which can be implemented in parallel in a Jacobian-free low-memory manner.

We consider DG Methods for the Euler equations and for viscous flow equations in 2D, both with gravity, in a well balanced formulation. Numerical experiments in the software framework DUNE-FEM on atmospheric flow problems show the benefit of this approach.

Keywords: DG, FV, implicit, multigrid, preconditioner, Jacobian-free, numerical weather prediction, DUNE, DUNE-FEM

1 Introduction

Discontinuous Galerkin methods has emerged as one of the most promising discretizations to replace second order finite volume methods for simulations of turbulent, time dependent, compressible fluid flow.

- It is of high order, a property of critical importance for efficient Large-Eddy-Simulation (LES) of turbulent flows.
- It can handle the complex geometries necessary in real world applications.
- It has computational advantages on modern computer architectures, and lends itself well to parallelization

In this article, we make use of Discontinuous Galerkin methods (DG) on quadrilateral grids. However, the techniques developed here can be used with other DG formulations as well, for example, Discontinuous Spectral Element methods (DG-SEM) where use is made of a tensor product extension from a one dimensional formulation or other general DG methods on simplicial grids.

Many applications require implicit time stepping to avoid excessive time step restrictions. This is the case when the mesh size varies considerably within the domain, or when the phenomena of interest to occur over long time scales compared to the fastest dynamics. The former occurs in particular when high aspect ratio grids are employed, as is the case for wall bounded viscous flows, but also for atmospheric flows where the gravitational force requires finer resolution in the vertical direction. The latter is also a problem in numerical weather prediction (NWP). In particular, the fastest processes are sound waves travelling at the speed of sound, whereas the phenomena of interest travel at the flow velocity. For low Mach flows, as is often the case in NWP, this is a serious issue.

In this article, we will consider fully implicit time integration, which leads to one large global system of equations. Complementary approaches that we will not follow in this text, are implicit-explicit (IMEX) methods, and horizontal explicit, vertical implicit (HEVI) ones that have seen a lot of application in NWP [1, 2]. These make use of a geometric or term wise splitting of the equations and use different time integration methods for the different parts. The technique suggested here can be employed subsequently in those methods as well.

Implicit time stepping requires solving large sparse linear systems of equations, which in turn requires efficient solvers to be competitive computationally. As pointed out in [3], to achieve the peak floating point performance on modern processors, it is necessary to reuse data loaded into the CPU, i.e. the arithmetic intensity of the algorithms must be sufficiently high. Algorithms based on frequent matrix-vector products with assembled matrices are unlikely to achieve sufficient arithmetic intensity, and it is therefore necessary to consider matrix-free or Jacobian-free algorithms [4, 5] and preconditioners suitable for such solvers. The lack of efficient and grid independent solvers for DG discretizations of compressible time dependent flow problems limits

the applicability of high order discretizations in many practical applications. Previous attempts are for example [6–11]. Robust and efficient preconditioning techniques for Jacobian-free Newton-Krylov (JFNK) solvers are therefore an active area of research.

Multigrid methods have been shown to scale optimally in many settings, in particular for elliptic problems, but also for finite volume discretizations of compressible flows [12–14]. For the multigrid method to be Jacobian-free, the smoother must be Jacobian-free, restricting the possible choices. Recently, a new Jacobian-free multigrid preconditioner for use in JFNK methods was suggested in [15] and then extended in [16, 17]. The approach uses a geometric multigrid method defined on a sub cell finite volume discretization (also known as low-order-refined (LOR) preconditioning). It is therefore similar to p -multigrid, but allows to make use of existing smoothers for FV methods, such as [7, 18].

This motivates us to build on that foundation. We follow the framework from [19], which makes use of high order time integration, and a JFNK solver with a smart choice of tolerances. We extend the preconditioner named above to the discretized 2D viscous compressible flow equations with a source term for gravity, as is common for atmospheric flows. Thereby, we make use of the technique from [20] to obtain a well balanced scheme.

The paper is organized as follows. In Sections 2.1 and 2.2 we briefly recall the main building blocks of the DG discretization and implicit time stepping. In Sections 2.3 and 2.4.3 we introduce the proposed solver and preconditioner for DG discretizations. We then investigate in Section 3 the effectiveness of this approach for various atmospheric test cases.

2 Governing equations, Discretization and Solvers

We consider a general class of time dependent nonlinear advection-diffusion-reaction problems for a vector valued function $\mathbf{U}: (0, T) \times \Omega \rightarrow \mathbb{R}^r$ with $r \in \mathbb{N}^+$ components of the form

$$\partial_t \mathbf{U} = \mathcal{L}(\mathbf{U}) := -\nabla \cdot (F_c(\mathbf{U}) + F_v(\mathbf{U}, \nabla \mathbf{U})) \quad \text{in } (0, T] \times \Omega \quad (1)$$

in $\Omega \subset \mathbb{R}^d$, $d = 1, 2, 3$. Suitable initial and boundary conditions have to be added. F_c describes the convective flux, F_v the viscous flux, and S a source term. Note that all the coefficients in the partial differential equation are allowed to depend explicitly on the spatial variable x and on time t but to simplify the presentation we suppress this dependency in our notation.

For the discretization, we use a method of lines approach based on first discretizing the differential operator in space using a DG approximation, and then solving the resulting system of ODEs using a time stepping scheme.

2.1 Discontinuous Galerkin Discretization

Given a tessellation \mathcal{T}_h of the computational domain Ω with $\cup_{E \in \mathcal{T}_h} E = \Omega$ we denote with Γ_i the set of all intersections between two elements of the grid \mathcal{T}_h , and the set of all intersections, also with the boundary of the domain Ω , is denoted by Γ .

We consider a discrete space V_h^k spanned by Lagrange type basis functions $\psi_i(x)$ based on tensor product Gauss-Legendre (GL) quadrature nodes. This yields diagonal mass matrices as discussed in detail in [21–23].

After fixing the grid and the discrete space, we seek

$$\mathbf{U}_h(t, x) = \sum_i \mathbf{U}_i(t) \psi_i(x) \in V_h^k,$$

by discretizing the spatial operator $\mathcal{L}(\mathbf{U})$ in (1) with boundary conditions by defining for all test functions $\boldsymbol{\psi} \in V_h^k$,

$$\langle \boldsymbol{\psi}, \mathcal{L}_h(\mathbf{U}_h) \rangle := \langle \boldsymbol{\psi}, K_h(\mathbf{U}_h) \rangle + \langle \boldsymbol{\psi}, I_h(\mathbf{U}_h) \rangle. \quad (2)$$

Hereby, we have the element integrals

$$\langle \boldsymbol{\psi}, K_h(\mathbf{U}_h) \rangle := \sum_{E \in \mathcal{T}_h} \int_E ((F_c(\mathbf{U}_h) - F_v(\mathbf{U}_h, \nabla \mathbf{U}_h)) : \nabla \boldsymbol{\psi} + S(\mathbf{U}_h) \cdot \boldsymbol{\psi}), \quad (3)$$

and the surface integrals (by introducing appropriate numerical fluxes H_c, H_v for the convection and diffusion terms, respectively)

$$\begin{aligned} \langle \boldsymbol{\psi}, I_h(\mathbf{U}_h) \rangle := & \sum_{e \in \Gamma_i} \int_e (\{F_v(\mathbf{U}_h, [\mathbf{U}_h]_e)^T : \nabla \boldsymbol{\psi}\}_e + \{F_v(\mathbf{U}_h, \nabla \mathbf{U}_h)\}_e : [\boldsymbol{\psi}]_e) \\ & - \sum_{e \in \Gamma} \int_e (H_c(\mathbf{U}_h) - H_v(\mathbf{U}_h, \nabla \mathbf{U}_h)) : [\boldsymbol{\psi}]_e, \end{aligned} \quad (4)$$

with $\{\mathbf{U}\}_e, [\mathbf{U}]_e$ denoting the classic average and jump of \mathbf{U} over $e \in \Gamma$, respectively. The convective numerical flux H_c is chosen to be the HLLC flux (see [24] for details).

A wide range of diffusion fluxes H_v can be found in the literature and many of these fluxes are available in DUNE-FEM-DG, for example, Interior Penalty and variants, Local DG, Compact DG 1 and 2 as well as Bassi-Rebay 1 and 2 (cf. [25, 26]).

We then require the Galerkin condition

$$\frac{d}{dt} \int_{\Omega} \mathbf{U}_h \cdot \boldsymbol{\psi} \, dx = \langle \boldsymbol{\psi}, \mathcal{L}_h(\mathbf{U}_h) \rangle \quad (5)$$

for all test functions $\boldsymbol{\psi} \in V_h^k$.

2.2 Temporal discretization

Equation (5) is a system of ODEs for the coefficients of $\mathbf{U}(t)$ which reads

$$\mathbf{U}'(t) = f(\mathbf{U}(t)) \text{ in } (0, T] \quad (6)$$

with $f(\mathbf{U}(t)) = M^{-1}\mathcal{L}_h(\mathbf{U}_h(t))$ where the mass matrix M is given element wise by

$$m_{ij} = \int_E \varphi_i \varphi_j = \omega_i \delta_{ij}.$$

The initial value $\mathbf{U}(0)$ is given by the L_2 projection of \mathbf{U}_0 onto V_h^k .

We use Singly-Diagonally Implicit Runge Kutta (SDIRK) methods because of their simplicity and relatively low cost compared to fully implicit schemes. A SDIRK method is defined by a lower triangular Butcher tableau with constant nonzero diagonal elements. In every stage, a nonlinear equation system of the form

$$\mathbf{G}(\mathbf{U}_s) := \mathbf{U}_s - \alpha \Delta t f(\mathbf{U}_s) - \bar{\mathbf{U}}_s = \mathbf{0} \quad (7)$$

is to be solved, where U_s is the stage value at stage s . \bar{U}_s and α are the previous stage value and the diagonal entry in the Butcher tableau.

Specifically, we use a method of order 2 with 2 stages known as Ellsiepen's method (8), or SDIRK2, with $\alpha = 1 - \frac{\sqrt{2}}{2}$, see [27].

2.3 Solver

The systems (7) are solved using a preconditioned Jacobian-free Newton-Krylov method (see [28]). The preconditioning strategy is the main topic of this article. We use a multi-grid preconditioner based on a low order discretization of the problem.

Newton's method is applied to solve (7) with initial guess $\mathbf{U}_s^0 = \bar{\mathbf{U}}_s$:

$$\mathbf{G}'(\mathbf{U}_s^k) \delta \mathbf{U}_s = -\mathbf{G}(\mathbf{U}_s^k), \quad (9)$$

$$\mathbf{U}_s^{k+1} = \mathbf{U}_s^k + \delta \mathbf{U}_s. \quad (10)$$

The iteration is terminated when

$$|\mathbf{G}(\mathbf{U}_s^k)| < \text{TOL} |\mathbf{G}(\mathbf{U}_s^0)| \quad (11)$$

where TOL is a specified tolerance. The linear system (9) is solved using GMRES with a preconditioner based on a multigrid method, which will be explained in the following subsections. The tolerance for the termination of the Krylov method is selected adaptively using the second Eisenstat-Walker criterion [29] (setting the parameters $\gamma = 0.1$ and $\alpha = 1$).

GMRES is used in a Jacobian-free manner, i.e. using a finite difference approximation of the Jacobian-Vector product, to avoid the storage of large Jacobian matrices, which for higher order DG methods are prohibitively large:

$$\mathbf{G}'(\mathbf{U})\mathbf{y} \approx \frac{1}{\epsilon} \left[\mathbf{G}(\mathbf{U} + \epsilon \mathbf{y}) - \mathbf{G}(\mathbf{U}) \right], \quad (12)$$

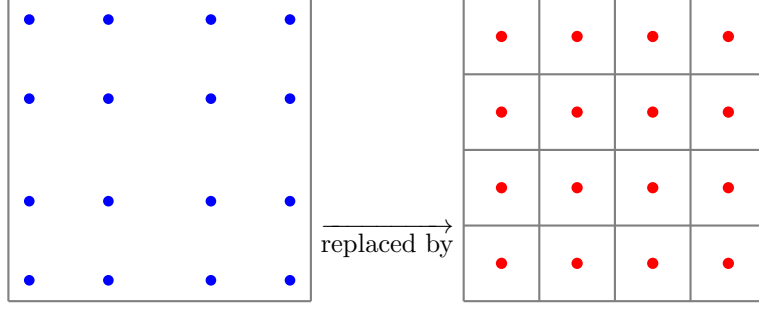


Fig. 1: (Left) Gauß-Legendre (GL) nodes for $k = 3$ in one grid cell and (right) FV cell averages in subgrid. The specific position of interpolation nodes for the DG method is only of interest for DG-SEM variants.

where $\epsilon = \sqrt{\epsilon_{mach}}/|\mathbf{y}|$ and ϵ_{mach} is the machine precision.

2.4 Low order approximation preconditioner

The main difficulty here now lies in finding an effective Jacobian-free preconditioner. The setup excludes some common options such as Gauss-Seidel or incomplete LU preconditioners. Instead we choose a geometric agglomeration multigrid preconditioner based on an auxiliary low order discretization of the problem, described in [15, 16].

We make use of a finite volume discretization, defined by the description in Section 2.1 with polynomial degree $k = 0$. It is defined on a subgrid of the DG grid in such a way that the two discretizations have the same number of degrees of freedom. The low order spatial discretization on the refined grid defines a function space V_h^0 consisting of piece-wise constant functions and an operator f_{low} , such that the low order spatial discretization of the problem reads

$$\mathbf{u}'(t) = f_{low}(\mathbf{u}(t)), \quad (13)$$

where \mathbf{u} is the corresponding vector of the degrees of freedom. An example of a subgrid using an equidistant subdivision is shown in Figure 1 for a DG space of order three.

Using the same temporal discretization as for the high order problem, the spatially low order discretization gives rise to a nonlinear system corresponding to eqn. (7)

$$\mathbf{g}(\mathbf{u}_s) := \mathbf{u}_s - \alpha \Delta t f_{low}(\mathbf{u}_s) - \bar{\mathbf{u}}_s = \mathbf{0}, \quad (14)$$

and the linear system

$$\mathbf{g}'(\mathbf{u}_s^k) \delta \mathbf{u}_s = -\mathbf{g}(\mathbf{u}_s^k) \quad (15)$$

corresponding to eqn. (9).

Assuming we have a preconditioner $\mathbf{q}^{-1}(\mathbf{u}_s^k) \approx \mathbf{g}'(\mathbf{u}_s^k)^{-1}$ for (15), we define a preconditioner for eqn. (9) to be

$$\mathbf{Q}^{-1} := \mathbf{T}^{-1} \mathbf{q}^{-1} \mathbf{T}, \quad (16)$$

where \mathbf{T} is a *transfer function* between the two discretizations (see Section 2.4.1). Note that the transfer function can also be combined with a pre or post smoothing step, which is discussed in Section 2.4.3.

2.4.1 Transfer functions

We now define mappings between the degrees of freedom of the high and the low order discretization. The vectors $\mathbf{U}_s, \mathbf{U}_s^k, \bar{\mathbf{U}}_s$ in the original discretization represent functions in V_h^k . Correspondingly, $\mathbf{u}_s, \mathbf{u}_s^k, \bar{\mathbf{u}}_s$ represent solutions of the low order discretization, i.e. functions in V_h^0 . The transfer functions between V_h^k and V_h^0 are defined such that the functions are close *in some sense*.

An obvious choice for \mathbf{T} would be the L^2 projection. However, in our experience, the simpler mapping of interpolating the polynomials in V_h^k in the cell centers of the cells defining V_h^0 gives the same preconditioner performance, while being much easier to implement on unstructured grids and requiring less computational cost. A detailed comparison of different approaches shows the interpolation based transfer functions offer the best performance in terms of preconditioner iterations and computing time [16, 30] and was therefore chosen for the experiments in this paper. Further discussions on this topic can be found in [31].

2.4.2 Conservation of mass

For the operator in (16) to conserve mass, both the low order preconditioner and the transfer function have to do so. See [32, 33] for a discussion on mass conservation of iterative methods and preconditioners. If the transfer function is based on L_2 projection, it conserves mass, but the interpolation introduces small conservation errors. If the problem at hand is sensitive to mass change, it is possible to add a *mass fix* to make the transfer function mass conservative.

The mass fix adds a term to the interpolation transfer function that is the average of the mass difference between the high order and the low order approximation in every DG cell:

$$\mathbf{T}_E^{mf} \mathbf{u} := \mathbf{T}_E \mathbf{u} - \frac{(m_E(\mathbf{T}_E \mathbf{u}) - m_E(\mathbf{u}))}{|E|} \mathbf{1}. \quad (17)$$

Here, \mathbf{T}_E is the block of \mathbf{T} relevant to the grid cell E and $m_E(\cdot) = \int_E \cdot$ is the mass in cell E . For the low order approximation given by $\mathbf{T}_E \mathbf{u}$, this is straightforward to compute.

For the high order approximation \mathbf{u} , it is possible to avoid evaluating this function in the DG nodes as well. To this end, the evaluations at the cell centers of the finite volume cells can be reused by using suitable quadrature weights such that these form a quadrature of the correct order. These weights are listed in the Appendix for $k = 3$.

For the test cases in this article we observed no difference between the interpolation transfer function and the mass fix interpolation transfer function in terms of preconditioner efficiency or quality of the solution.

2.4.3 Multigrid preconditioner for finite volume approximations

We start with a sequence of increasingly refined quad meshes \mathcal{T}_l for $l = 0 \dots L$, where \mathcal{T}_l is generated by splitting each quad $E \in \mathcal{T}_{l-1}$ into 2^d new child quads denoted by $C(E)$. The approximation on level l is represented by a vector \mathbf{U}_l .

The method is defined by choosing restriction and prolongation operators, \mathbf{R} , \mathbf{P} , and a *smoother*, $\mathbf{S}(\cdot, \cdot)$.

For the restriction \mathbf{R} we use the agglomeration restriction, mapping the cell averages on the quads $C(E)$ of the fine tessellation \mathcal{T}_l to the volume averaged cell average on quad E of the coarser tessellation \mathcal{T}_{l-1} :

$$(\mathbf{R}\mathbf{U}_l)_E = \frac{1}{|E|} \sum_{q \in C(E)} |q| U_{l,q}, \quad \forall E \in \mathcal{T}_{l-1}. \quad (18)$$

For prolongation we use the injection operator \mathbf{P} . It assigns the cell average of the agglomerate to all split quads. It can be expressed as

$$(\mathbf{P}\mathbf{U}_l)_q = U_{l,E}, \quad \forall q \in C(E), \quad E \in \mathcal{T}_l. \quad (19)$$

The smoother $\mathbf{S}(\cdot, \cdot)$ is a linear iterative method that converges to the solution of (15). It is designed to quickly reduce high frequency components of the error. We use a smoother based on pseudo time iteration, described in section 2.4.4.

The multigrid algorithm consists of a V- or W-cycle with pre- and post-smoothing. On the coarsest grid level we apply the smoother twice. The multigrid algorithm for solving equation (15) can be written as

1. Compute $\mathbf{MG}_l(\mathbf{x}, \mathbf{b}; \mathbf{u}_s^k)$:
2. $\mathbf{x} := \mathbf{S}(\mathbf{x}, \mathbf{b})$
3. If $l > 0$
 - $\mathbf{r} := \mathbf{R}(\mathbf{g}'(\mathbf{u}_s^k)\mathbf{x} - \mathbf{b})$
 - $\mathbf{v} := \mathbf{0}$
 - Repeat once for V-cycle and twice for W-cycle
 - $\mathbf{v} := \mathbf{MG}_{l-1}(\mathbf{v}, \mathbf{r}; \mathbf{R}\mathbf{u}_s^k)$
 - $\mathbf{x} := \mathbf{x} - \mathbf{P}\mathbf{v}$
4. $\mathbf{x} := \mathbf{S}(\mathbf{x}, \mathbf{b})$
5. Return \mathbf{x}

The preconditioner is obtained by calling this routine with initial guess $\mathbf{x} = \mathbf{0}$. To make this efficient, we add a flag that avoids MatVecs with the zero vector.

2.4.4 Smoother / Pseudo time iteration

A common approach to solve linear systems such as (15) arising from computational fluid dynamics models is so called pseudo-time stepping. Smoothing can be both done during the multigrid cycle, i.e., on the finite-volume data before or after prolongation/restriction. Smoothing is also possible on the DG data before the transfer to the finite-volume grid or after reconstruction of the DG data. In both cases we use a similar pseudo-time stepping approach which we describe here only for the finite-volume data.

Instead of solving (15) directly, a pseudo time variable is introduced

$$\frac{\delta \mathbf{w}}{\delta \tau} = -\mathbf{g}(\mathbf{u}_s^k) - \mathbf{g}'(\mathbf{u}_s^k)\mathbf{w} \quad (20)$$

to construct an ODE with a steady state at the solution of the linear system. The ODE is stable if the original spatial discretization of the system is stable. In the next step, an explicit Runge-Kutta (ERK) time integration scheme is used to integrate in pseudo time from an initial guess, namely the current approximation \mathbf{x} in the pseudocode.

These methods have several parameters, namely Runge-Kutta coefficients and a time step in pseudotime, Δt^* . The latter is computed based on a pseudo CFL number. This means that on coarser grids, larger time steps will be taken. These are chosen based on [18]. There, the parameters are optimized for certain physical CFL numbers. In the experiments, the smoother is the one stage explicit Euler scheme, which we found to be the most efficient.

3 Numerical Experiments

The governing equations for the test cases are two dimensional viscous compressible flow equations. Expressed as in Eq. (1) they are given by

$$F_c(\mathbf{U}) = \begin{bmatrix} \rho u & \rho w \\ \rho u^2 + p & \rho uw \\ \rho uw & \rho w^2 + p \\ u\rho\theta & w\rho\theta \end{bmatrix}, \quad F_v(\mathbf{U}, \nabla \mathbf{U}) = \mu\rho \begin{bmatrix} \mathbf{0} \\ \nabla u \\ \nabla w \\ \nabla \theta \end{bmatrix}, \quad S_i(\mathbf{U}) = \begin{bmatrix} 0 \\ 0 \\ -\rho g \\ 0 \end{bmatrix}, \quad (21)$$

with $S_e(\mathbf{U}) = \mathbf{0}$ in the test cases if nothing else is specified. If the diffusion term is neglected, one recovers the Euler equations with a gravity source term. These will be use for several of the test cases.

It is common for atmospheric test cases to consider a perturbation of a *environmental atmosphere*, i.e., a stationary solution $\bar{\mathbf{U}} = (\bar{\rho}, \bar{\rho}\bar{\mathbf{v}}, \bar{\rho}\bar{\theta})$, which fulfill (21) with $\mu = 0$. To avoid numerical errors in balancing the environmental atmosphere from polluting the simulation results, we use the well-balancing scheme introduced in [34], which is based on applying our DG method to the system for the perturbations \mathbf{U}' :

$$\partial_t \mathbf{U}' + \nabla \cdot (F_c(\mathbf{U}' + \bar{\mathbf{U}}) - F_c(\bar{\mathbf{U}}) - F_v(\mathbf{U}' + \bar{\mathbf{U}}, \nabla(\mathbf{U}' + \bar{\mathbf{U}}))) = S_i(\mathbf{U}' + \bar{\mathbf{U}}) - S_i(\bar{\mathbf{U}}). \quad (22)$$

To apply DG to (22), we rewrite the equation as

$$\partial_t \mathbf{U}' + \nabla \cdot (F_c^{pert}(\mathbf{U}') - F_v^{pert}(\mathbf{U}')) = S^{pert}(\mathbf{U}')$$

with

$$F_c^{pert}(\mathbf{U}') = F_c(\mathbf{U}' + \bar{\mathbf{U}}) - F_c(\bar{\mathbf{U}}), \quad F_v^{pert}(\mathbf{U}') = F_v(\mathbf{U}' + \bar{\mathbf{U}}, \nabla(\mathbf{U}' + \bar{\mathbf{U}})), \\ S_i^{pert}(\mathbf{U}') = S_i(\mathbf{U}' + \bar{\mathbf{U}}) - S_i(\bar{\mathbf{U}}),$$

and apply the DG procedure as described in Section 2.1. The corresponding numerical fluxes $\hat{F}_c^{pert}(\mathbf{U}')$ and $\hat{F}_v^{pert}(\mathbf{U}')$ now read

$$\hat{F}_c^{pert}(\mathbf{U}') = \hat{F}(\mathbf{U}' + \bar{\mathbf{U}}) - \hat{F}(\bar{\mathbf{U}}), \quad \hat{F}_v^{pert}(\mathbf{U}') = \hat{F}_v(\mathbf{U}' + \bar{\mathbf{U}}, \nabla(\mathbf{U}' + \bar{\mathbf{U}})).$$

Applying the DG method to (22) guarantees that $\mathbf{U}' \equiv 0$ is maintained on the discrete level, if \mathbf{U}' vanishes initially. Furthermore, this version of the system has significant advantages in adaptive computations as shown in [20]. Notice that this approach requires that the environmental atmosphere is given a-priori.

In all tests we compute a DG solution based on tensor product Legendre polynomials of degree $k = 3$ on a given refinement level l of a cartesian grid. The multigrid preconditioner then uses $l + 2$ levels since going from DG with order $k = 3$ to the finest FV grid adds two level as shown in Figure 1. To test the effectiveness of the multigrid preconditioner we use an implicit SDIRK2 with a fixed time step Δt and fixing a relatively coarse tolerance of $\text{TOL} = 10^{-3}$ for the Newton method if not mentioned otherwise. For the linear solver we use a matrix free GMRES method where the tolerance is selected adaptively using the second Eisenstat-Walker criterion as mentioned previously. We then compare the number of iterations of the GMRES solver for the non preconditioned and different multigrid setups.

For the preconditioner there are a variety of configuration parameters which are encrypted in the following key for our experiments:

$$\mathbf{mg} a b c d e f G \tag{23}$$

The **mg** is an abbreviation for multigrid and the other letters have the following meaning:

- a, b : Number of **pre** and **post** smoothing steps on the DG solution
- c, d : Number of **pre** and **post** smoothing steps on the finest FV level
- e, f : Number of **pre** and **post** smoothing steps on the intermediate FV levels
- G : Either **V** or **W**, denoting the cycle of the multigrid method

For example, the configuration **mg111111V** means multigrid in V-cycle mode with one pre and post smoothing step on the DG solution as well as on all FV levels.

To obtain a reference solution, we in addition include results for an explicit 4-stage 3rd order SSP method described in [35] and implemented in DUNE-FEM-DG [21] with a time step Δt close to the stability limit of the explicit method.

3.1 Non-hydrostatic inertia gravity

This test case, introduced in [36], considers the evolution of a potential temperature perturbation. The perturbation is so small that the bubble does not have enough buoyancy to rise, but rather oscillates in the vertical direction, creating a specific wave like pattern in the horizontal direction. The domain is a tube of dimension $[0, 300\,000] \times [0, 10\,000] \text{km}^2$. The given environmental atmosphere has constant Brunt-Väisälä frequency $N = 10^{-2} \text{ s}^{-1}$, the surface pressure $p_0 = 10^5 \text{Pa}$, the surface temperature $T_0 = 250\text{K}$, and a constant mean flow $\tilde{u} = 20\text{m/s}$ and $\tilde{w} = 0$.

The governing equations for this test case are the Euler equations with gravity source term. The potential temperature, temperature and pressure values of the environmental atmosphere are given by

$$\tilde{\theta}(x, z) = T_0 \exp \frac{z}{H}, \quad (24)$$

$$\tilde{T}(x, z) = T_0 \left(\alpha - (\alpha - 1) \exp \frac{z}{H} \right), \quad (25)$$

$$\tilde{p}(x, z) = p_0 \exp \left(\frac{c_p}{R_d} \left(\ln \frac{\tilde{T}}{T_0} - \frac{z}{H} \right) \right) \quad (26)$$

with constants H and α defined as

$$H = \frac{g}{N^2}, \quad \alpha = \frac{gH}{c_p T_0}. \quad (27)$$

For this test case, we choose $c_p = 1.005\text{J}/(\text{kg K})$, $c_v = 717.95\text{J}/(\text{kg K})$, and $g = 9.80665\text{m}/\text{s}^2$.

The initial perturbation of the potential temperature is given by

$$\theta'(x, z) = \theta_c \left(1 + \left(\frac{x - x_c}{a} \right)^2 \right)^{-1} \sin \frac{\pi z}{Z}, \quad (28)$$

with $Z = 10^4\text{m}$ preserving the pressure values. The maximal deviation from the stratified atmosphere $\theta_c = 0.01\text{K}$, the center of the perturbation bubble on the x-axis $x_c = 100,000\text{m}$, and $a = 5,000\text{m}$. Introducing the perturbation θ' of the potential temperature into the environmental atmosphere while preserving pressure finally defines the initial state $\mathbf{U} = (\rho, \rho\mathbf{v}, \rho\theta)$ through

$$\rho = \frac{p_0^{R_d/c_p} \tilde{p}^{\frac{1}{\gamma}}}{R_d(\tilde{\theta} + \theta')}, \quad \mathbf{v} = \tilde{\mathbf{v}}, \quad \theta = \tilde{\theta} + \theta'. \quad (29)$$

Periodic boundary conditions are imposed on the lateral boundaries, whereas slip boundary conditions are assumed elsewhere. The Euler equations with the prescribed initial and boundary data are integrated until 3,000s of the model time in order to obtain a solution for comparison. If not mentioned otherwise the simulations are carried out on a twice refined equally spaced grid resulting in a spatial resolution of around $\Delta x = 940\text{m}$.

Figure 2 shows the potential temperature perturbation at the final time using the implicit method with time steps $\Delta t = 25, 50, 100$ together with a reference solution obtained with the explicit method using $\Delta t = 0.028$. The implicit methods are thus using time steps which are around 1,000 to 4,000 times the stable time step of the explicit method. The results look still fairly similar although in the center some detail is lost when using very large time steps. This is clearly visible in Figure 3 where the solutions are plotted along the height $y = 5,000$. While the results with $\Delta t = 25$ still broadly follow the reference solution there is some clearer deviation when even larger

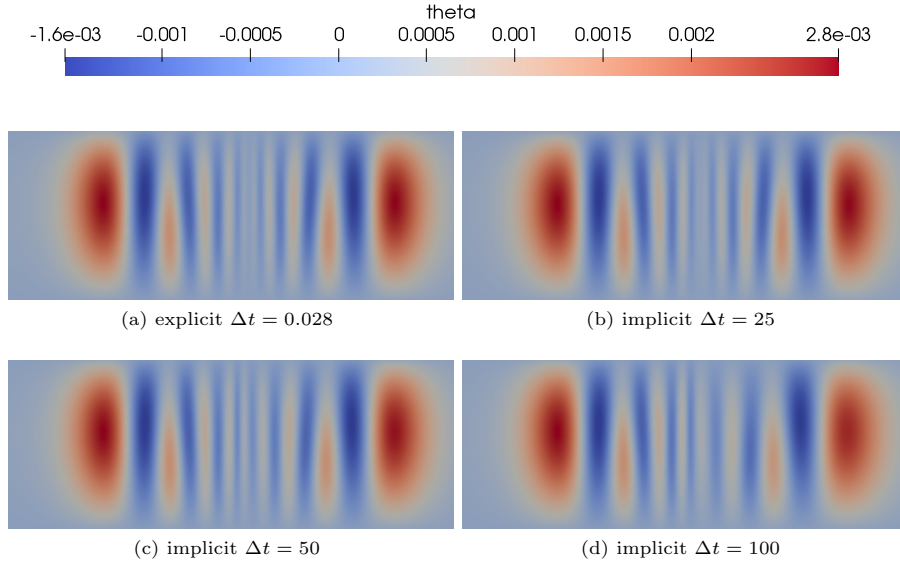


Fig. 2: Inertia Gravity test case: perturbation in the potential temperature θ at the final time $T = 3000$ for $\Delta x = 940\text{m}$ using implicit solvers with different time steps and an explicit solver (top left).

time are being used. Figure 4 shows the same cut using time steps $\Delta t = 6.75, 12.5, 25$. It is clear that the results with $\Delta t = 12.5$ which is about 500 times the time step used in the explicit simulation are very close to the reference solution.

To investigate the efficiency of the multigrid preconditioner, we show the number of iterations needed in each time step in Figure 5. The figure on the left are for the same resolution ($\Delta x = 940\text{m}$) used in the previous plots. One can see that the number of iterations scales sublinearly with increase in Δt between $\Delta t = 12.5$ and $\Delta t = 25$ while approximately twice the number of iterations are needed when going from $\Delta t = 25$ to $\Delta t = 50$ indicating that Δt around 25 is a good choice for this test case, i.e., about 500 times the explicit time step. In the center plot of Figure 5 we reduced the spatial resolution to around 470m by increasing the level to $\Delta x = 470\text{m}$. We used a time step of $\Delta t = 50$ and in addition $\Delta t = 100$ with two different parameter sets for the multigrid method. Again a below linear increase in the number of iterations can be seen. In addition the results indicate that the number of iterations can be reduced by up to 20% by including pre and post smoothing steps, although it should be noted that these do increase the computational cost of each iteration step. The more detailed discussion of the choice of the multigrid parameters is carried out for the next test case. Finally, in Figure 5c we compare the implicit method with and without our multigrid preconditioner. The number of iterations is significantly reduced by our method to the point that with a smaller tolerance in the Newton solver the simulation without preconditioning exceeded the time slot available on the supercomputer.

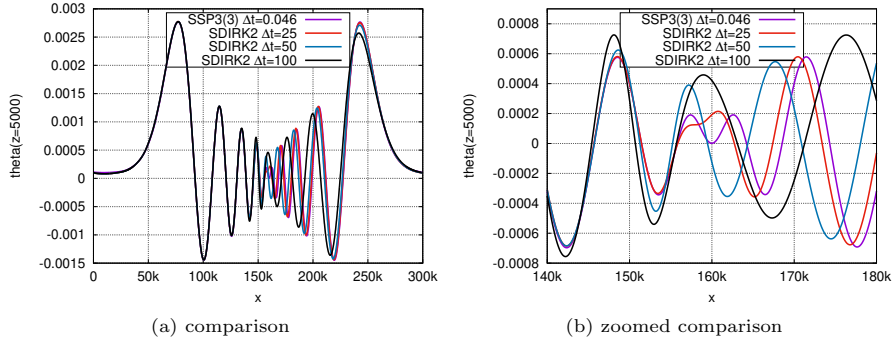


Fig. 3: Inertia Gravity test case: perturbation in the potential temperature θ at the final time $T = 3000$, $\Delta x = 940\text{m}$ at $z = 5,000\text{m}$. The same time steps are used as in Figure 2. The solution with the explicit method in blue acts as a reference solution. The right figure shows θ around the center of the domain, results along the full range of x is shown on the left.

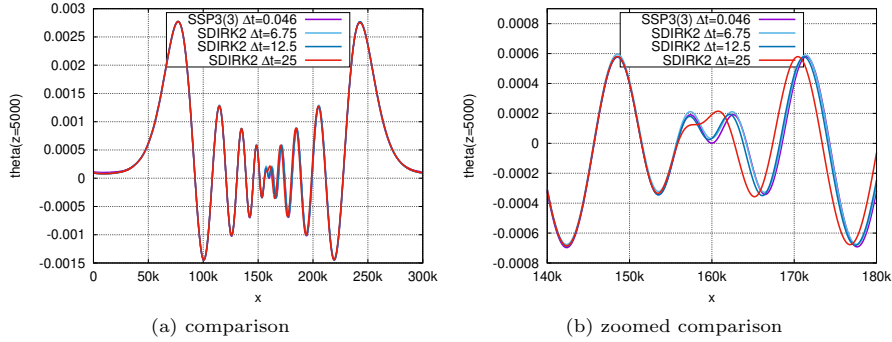


Fig. 4: Inertia Gravity test case: perturbation in the potential temperature θ at the final time $T = 3000$, $\Delta x = 940\text{m}$ at $z = 5,000\text{m}$. Smaller time steps are shown compared to Figure 3.

3.2 Rising warm air bubble

The setup for the evolution of a warm bubble in a neutrally stratified atmosphere follows the description in [37]. The bubble, positioned at a certain height, will start to rise and develop vortex structures in interaction with the cooler surrounding air. The stiffness in this test case comes from the difference in speed between the rising bubble and the fast sound waves also present in the solution.

The governing equations are the compressible Euler equations with gravitational force. The domain is $[0, 1000] \times [0, 2000]\text{m}^2$ and the environmental atmosphere is

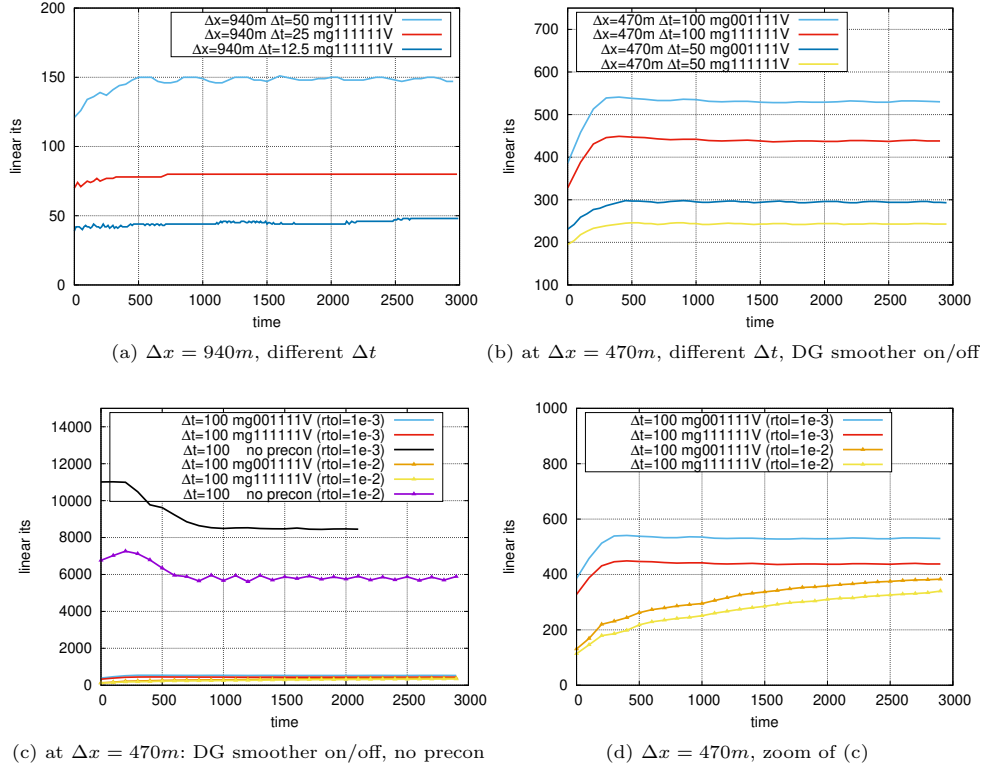


Fig. 5: Inertia Gravity test case: plots show the cumulative number of linear iterations needed to solve the non linear system in each time step over simulation time. Results with different values for the time step Δt are shown with the plot on the left showing results for $\Delta x = 940m$ while the other two plots show results with $\Delta x = 470m$. Different choices of the multigrid parameters are compared including on the right results without preconditioning.

determined by the formulas

$$\tilde{\theta} = 303.15K, \quad \tilde{T} = T_0 - zg c_p^{-1}, \quad \tilde{p} = p_0(\tilde{T}T_0^{-1})^{c_p/R_d}. \quad (30)$$

In the test case, $c_p = 1,005J/(kg K)$, $c_v = 717.95J/(kg K)$ and $g = 9.80665m/s^2$. The initial atmosphere is the sum of this neutrally stratified environmental atmosphere and a perturbation induced by a deviation of the potential temperature with the shape of a "flattened" Gaussian pulse, given by

$$\theta'(x, z) = A_0 \begin{cases} 1.0, & r := \|(x, z) - (x_0, z_0)\| < a, \\ \exp(-(r - a)^2/s^2), & 0 \leq r - a \leq 3s, \\ 0, & \text{else,} \end{cases} \quad (31)$$

where $A_0 = 0.5K$, $x_0 = 500m$, $z_0 = 520m$, $a = 50m$ and $s = 100m$. The introduction of the perturbation θ' into the initial state follows the approach described in [38]. On all sides of the domain we impose slip boundary conditions. The system is integrated until 1200s of model time.

For the runs at $\Delta x = 25m$ we the DG solution is computed on level $l = 2$ and for $\Delta x = 12.5m$ we have $l = 3$, which means 4 or 5 multigrid levels, respectively. For the simulations using the implicit SDIRK2 method, we use a fixed time step of $\Delta t = 5s$ and $\Delta t = 10s$. Other time step sizes have been tested but did yielded inferior results. The stable time step for the explicit method with a vertical resolution of $\Delta x = 12.5m$ was $\Delta t = 0.002558s$. The solution of the test case at various points in time for the explicit and one of the considered implicit configurations is displayed in Figure 6.

Figure 7 contains a selection of different configurations of the multigrid method for two time step sizes. In Figure 7a we compare the non-preconditioned implicit method with the preconditioned method. The different configurations include either no pre and post smoothing step on the DG solution and a mix of both, one or two smoothing steps on the FV levels as well as using a V-cycle and a W-cycle. The two best configurations in terms of minimal linear iterations and minimal CPU time are **mg001111V** and **mg111111V**, where the additional pre and post smoothing on the DG solution reduces the number of linear iterations at the cost of more operator evaluations. In addition, a W-cycle configuration was tested, e.g. **mg111111W**, yielding a competitive number of linear iterations but the overall application of the multigrid method is much more expensive leading to doubling in run time.

In Figure 7b we compare the number of operator calls (DG and FV combined) for the different combinations from Figure 7a. We can observe that the number of operator calls follow closely the number of linear iterations. Therefore, the number of operator calls is not further considered in the following.

Figure 7c compares the two best configurations from Figure 7a and 7b for different grid width $\Delta x = 25m$ and $\Delta x = 12.5m$. The number of linear iterations is not grid independent but grows with decreasing grid width. However, in this particular case the growth is less than a factor of two which we consider acceptable given that the time step size was kept constant at $\Delta t = 5s$.

Finally, Figure 7d shows the linear iterations needed when using the non-preconditioned implicit version. The simulation terminated prematurely due to exceeding the allocated time window on the super computer.

In summary, at grid width $\Delta x = 12.5m$ the fastest run was **mg111111V** with 7915s to finish followed by **mg001111V** with 8166s, both using $\Delta t = 5s$. Compared to the explicit SSP3(4) time stepping, which needed 14000s, this is roughly twice as fast. All other multigrid configurations were slower, including those using a larger time step size. At $\Delta x = 25m$, using a time step size of $\Delta t = 10s$ the configuration **mg111111V** needed 1181s followed by **mg001111V** which 1196s. The explicit SSP3(4) time stepping took 1763s.

3.3 Density current

In [39], the density current test case was proposed. In this test case, one examines the evolution of a cold bubble in neutrally stratified atmosphere. The bubble is positioned

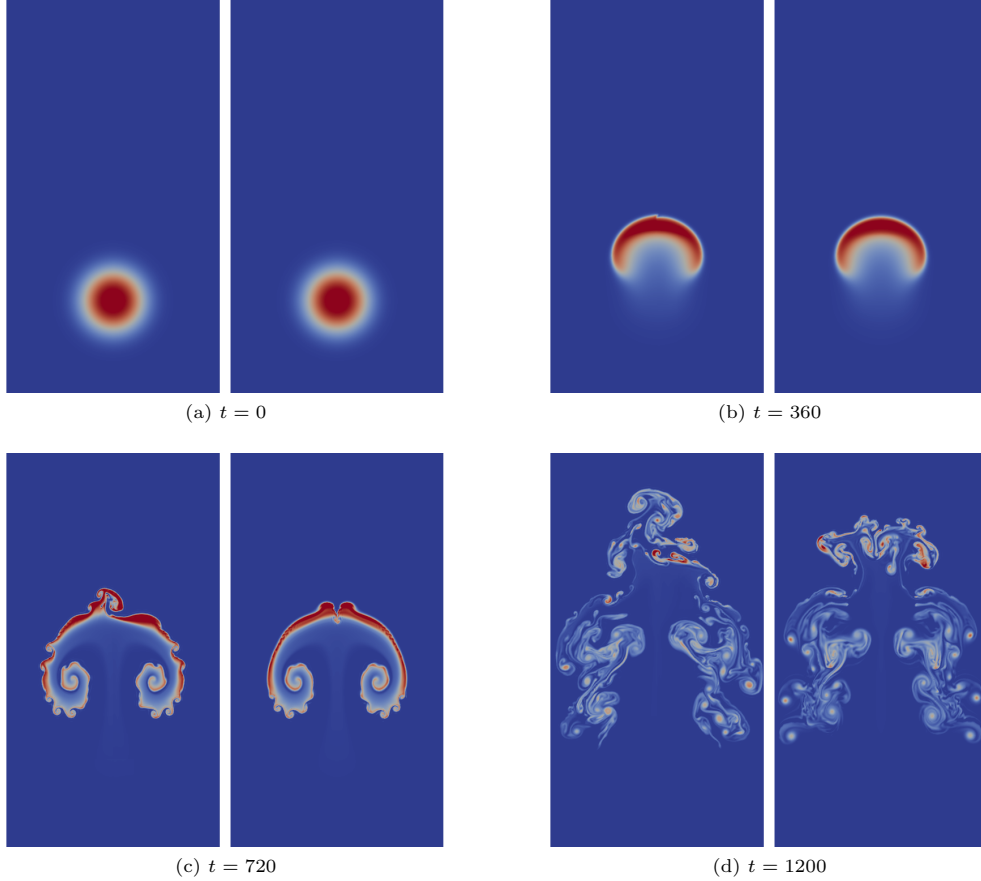


Fig. 6: Rising bubble test case: potential temperature perturbation at various times. Left, the solution computed at $\Delta x = 12.5m$ using the explicit time stepping with $\Delta t = 0.002558s$, and right the solution at $\Delta x = 12.5m$ using implicit time stepping with multigrid preconditioning and time step $\Delta t = 5s$. Note that the implicit time stepping allows to use a time step that is ≈ 2000 times larger than the explicit time step. Both schemes produce an acceptable solution.

at a certain height, and it will start to fall and eventually hit the ground. It will then slide along the ground level and create Kelvin-Helmholtz vortices. Approximately every 300s, a new Kelvin-Helmholtz vortex should appear. In order to obtain grid-convergent solutions, enough viscosity should be employed. In [38], the authors have discussed that setting $\mu = 75m^2/s$ is enough to obtain grid convergence. The setup of the initial conditions is as follows. The domain is $[0, 25,600] \times [0, 6,400]m^2$. The environmental atmosphere is determined by the formulas

$$\tilde{\theta} = 300K, \quad \tilde{T} = T_0 - zg c_p^{-1}, \quad \tilde{p} = p_0(\tilde{T}T_0^{-1})^{c_p/R_d}. \quad (32)$$

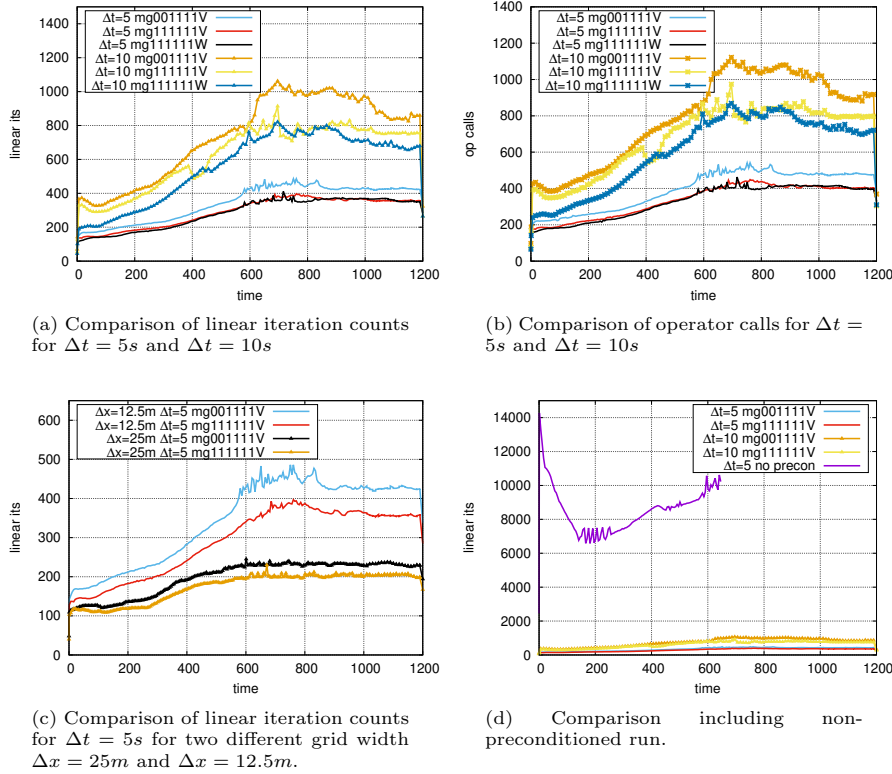


Fig. 7: Rising bubble test case: linear iterations for various configurations of the multigrid solver.

For this test case, we choose $c_p = 1,004\text{J}/(\text{kg K})$, $c_v = 717\text{J}/(\text{kg K})$, and $g = 9.81\text{m}/\text{s}^2$ as in [38, 39]. The initial data is a sum of this neutrally stratified environmental atmosphere and a perturbation field induced by the deviation of the potential temperature

$$\theta'(x, z) = \begin{cases} \frac{\theta_c}{2} (1 + \cos(\pi r(x, z))), & \text{for } r(x, z) < 1, \\ 0, & \text{else,} \end{cases} \quad (33)$$

where $\theta_c = -15\text{K}$ is the maximal deviation of the potential temperature from the stratified atmosphere, and r is the distance to the center of the perturbation bubble, given by

$$r^2(x, z) = ((x - x_c)/x_r)^2 + ((z - z_c)/z_r)^2. \quad (34)$$

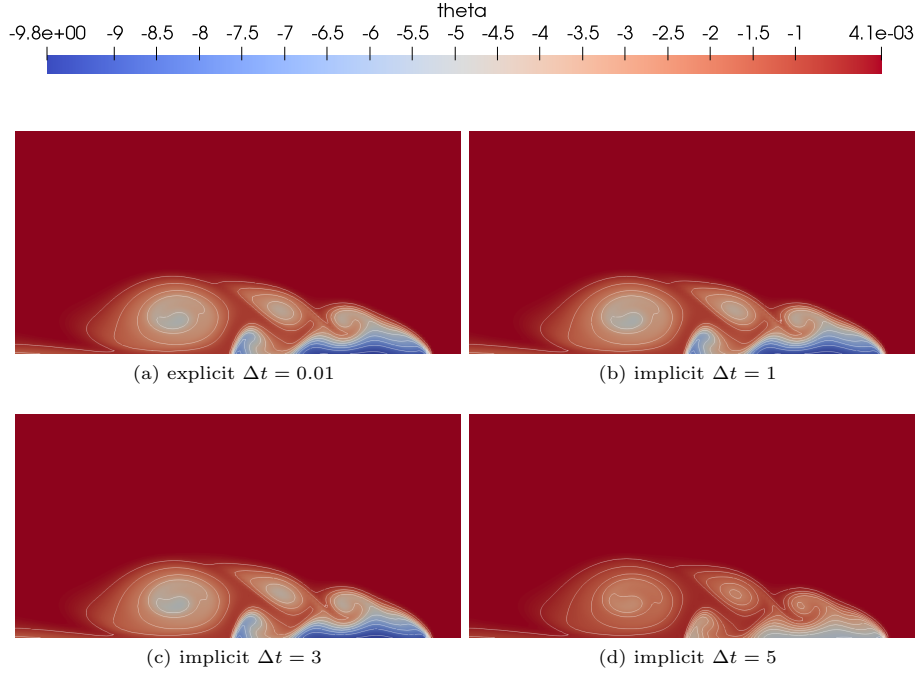


Fig. 8: Density current test case: perturbation in the potential temperature θ at the final time $T = 900$ for $\Delta x = 160\text{m}$ using implicit solvers with different time steps and an explicit solver (top left). The solution patterns corresponds to those reported in [38]. For $\Delta t = 5$ a deviation from the expected pattern is observed. Compare also with Figure 9.

The center of the perturbation bubble for the initial data is at $(x_c, z_c) = (0, 3,000)\text{m}$, with radii $x_r = 4,000\text{m}$ and $z_r = 2,000\text{m}$. The introduction of the perturbation θ' into the initial state follows the same way as in Eq. (29).

On all sides of the domain we impose slip boundary conditions (in spite of the fact that diffusion terms are present). The system is integrated until 900s of the model time.

In Figure 9 we can compare the performance of the implicit solver using different values for the time step Δt compared with a reference solution computed using the explicit method. Clearly using a 300 times larger time step compared to the stable time step needed in the explicit setting still results in a accurate solution. Close to a factor of 1,000 the solution shows some clear deviation not accurately resolving all the vortices. We conclude with again comparing the number of iterations needed with implicit solver using different time steps and different spatial resolutions in Figure 10. Results are similar to what we already observed with a sublinear growth in the number of iterations compared to increasing Δt . These results also indicate that for this test case there is only an increase of less then 50% in the number of iterations when the

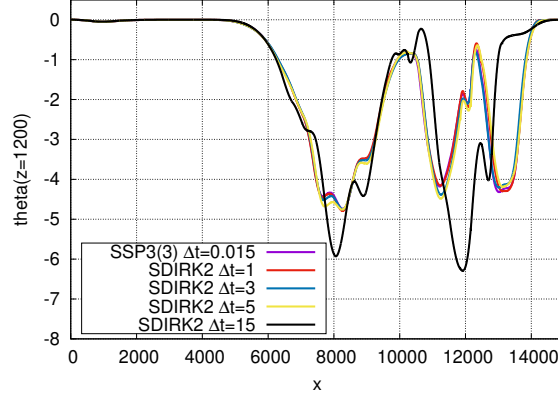


Fig. 9: Density current test case: solutions along the x -axis at $z = 1200\text{m}$ using different values of Δt . The solution using an explicit method is provided as reference solution. A good agreement can be observed up to and including $\Delta t = 3$.

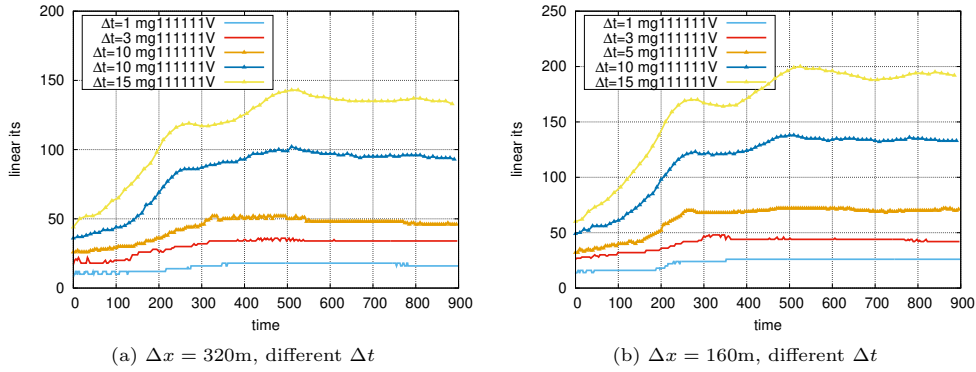


Fig. 10: Density current test case: plots show the cumulative number of linear iterations needed to solve the non linear system in each time step over simulation time. Results with different values for the time step Δt are shown using $\Delta x = 320\text{m}$ (left) and $\Delta x = 160\text{m}$ (right).

spatial resolution is increased. This is even less of an increase compared to the rising bubble test case.

At the finer resolution ($\Delta x = 160\text{m}$) the explicit time stepping scheme needs about 2734s to compute the solution at $T = 900$. The implicit scheme using the configuration `mg111111V` with $\Delta t = 3$ needed 1366s and 2580s for $\Delta t = 1$. At the coarser resolution ($\Delta x = 320\text{m}$) the implicit scheme was slower than the explicit scheme for all computed time step sizes.

4 Summary and Conclusions

We considered implicit time integration for parallel high order DG methods for compressible fluid flows. The arising systems are solved using a Jacobian-free Newton-GMRES solver with preconditioner. The preconditioner is based on a multigrid method for a first order finite volume discretization on an auxiliary mesh, based on the DG mesh. To transfer between the meshes in a computationally efficient manner, either a mass conservative L_2 mapping, or interpolation with a mass fix can be used. As smoothers, low-storage explicit Runge-Kutta pseudo time iterations are used, which are implemented in parallel in a Jacobian-free manner. The preconditioner is thus Jacobian-free, uses little extra memory, and achieves close to optimal arithmetic intensity for large problems on parallel machines.

The numerical experiments are performed in the software framework DUNE-FEM for three well known atmospheric test cases in 2D. These are a non-hydrostatic inertia gravity case, a rising bubble of warm air, and a density current test case. Gravity is incorporated in a well-balanced manner. The implicit high order solver produces accurate results even for large CFL numbers. For these, the unpreconditioned solver is prohibitively slow or does not converge at all. The preconditioner increases the stability of the solver while substantially reducing the number of iterations, making the implicit method competitive. On grids with higher resolution the preconditioned implicit solver becomes competitive in terms of run times compared to an explicit solver.

Conflict of interest

On behalf of all authors, the corresponding author states that there is no conflict of interest.

References

- [1] Bao, L., Klöforn, R., Nair, R.D.: Horizontally Explicit and Vertically Implicit (HEVI) Time Discretization Scheme for a Discontinuous Galerkin Nonhydrostatic Model. *Mon. Wea. Rev.* **143**, 972–990 (2015) <https://doi.org/10.1175/MWR-D-14-00083.1>
- [2] Giraldo, F.X., de Bragança Alves, F.A.V., Kelly, J.F., Kang, S., Reinecke, P.A.: A performance study of horizontally explicit vertically implicit (hevi) time-integrators for non-hydrostatic atmospheric models. *Journal of Computational Physics* **515**, 113275 (2024) <https://doi.org/10.1016/j.jcp.2024.113275>
- [3] Bastian, P., Müller, E., Müthing, S., Piatkowski, M.: Matrix-free multigrid block-preconditioners for higher order Discontinuous Galerkin discretisations. *J. Comput. Phys.* **394**, 417–439 (2019) <https://doi.org/10.1016/j.jcp.2019.06.001>
- [4] Kempf, D., Heß, R., Müthing, S., Bastian, P.: Automatic Code Generation for High-Performance Discontinuous Galerkin Methods on Modern Architectures.

- ACM Trans. Math. Softw. **47**(1) (2020) <https://doi.org/10.1145/3424144>
- [5] Kronbichler, M., Kormann, K.: Fast Matrix-Free Evaluation of Discontinuous Galerkin Finite Element Operators. ACM Trans. Math. Softw. **45**(3) (2019) <https://doi.org/10.1145/3325864>
- [6] Bassi, F., Ghidoni, A., Rebay, S., Tesini, P.: High-order accurate p-multigrid discontinuous Galerkin solution of the Euler equations. Int. J. Num. Meth. Fluids **60**, 847–865 (2009) <https://doi.org/10.1002/fld>
- [7] Birken, P., Gassner, G., Haas, M., Munz, C.D.: Preconditioning for modal discontinuous Galerkin methods for unsteady 3D Navier-Stokes equations. J. Comput. Phys. **240**, 20–35 (2013) <https://doi.org/10.1016/j.jcp.2013.01.004>
- [8] Carr, L.E., Borges, C.F., Giraldo, F.X.: Matrix-Free Polynomial-Based Nonlinear Least Squares Optimized Preconditioning and its Application to Continuous and Discontinuous Element-Based Discretizations of the Euler Equations. J. Sci. Comput. **66**, 917–940 (2016) <https://doi.org/10.1007/s10915-015-0049-9>
- [9] Franco, M., Persson, P.O., Pazner, W.: Iterative subregion correction preconditioners with adaptive tolerance for problems with geometrically localized stiffness. Commun. Appl. Math. Comput. **6**, 811–836 (2023) <https://doi.org/10.1007/s42967-023-00254-0>
- [10] Wang, L., Trojak, W., Witherden, F., Jameson, A.: Nonlinear p-Multigrid Preconditioner for Implicit Time Integration of Compressible Navier–Stokes Equations with p-Adaptive Flux Reconstruction. J. Sci. Comput. **93** (2022) <https://doi.org/10.1007/s10915-022-02037-w>
- [11] Puppo, G., Semplice, M., Visconti, G.: Quinpi: Integrating stiff hyperbolic systems with implicit high order finite volume schemes. Communications in Computational Physics **36** (2024) <https://doi.org/10.4208/cicp.OA-2023-0199>
- [12] Caughey, D.A., Jameson, A.: How Many Steps are Required to Solve the Euler Equations of Steady Compressible Flow: In Search of a Fast Solution Algorithm. AIAA Paper 2001-2673 (2001) <https://doi.org/10.2514/6.2001-2673>
- [13] Birken, P., Bull, J., Jameson, A.: Preconditioned Smoothers for the Full Approximation Scheme for the RANS Equations. J. Sci. Comput. **78**(2), 995–1022 (2019) <https://doi.org/10.1007/s10915-018-0792-9> arXiv:1710.04875
- [14] Birken, P.: Numerical Methods for Unsteady Compressible Flow Problems. CRC Press, Boca Raton (2021). <https://doi.org/10.1201/9781003025214>
- [15] Birken, P., Gassner, G.J., Versbach, L.M.: Subcell finite volume multigrid preconditioning for high-order discontinuous Galerkin methods. Int. J. Comput. Fluid Dyn. **33**(9), 353–361 (2019) <https://doi.org/10.1080/10618562.2019.1667983>

- [16] Kasimir, J. and Versbach, L. M. and Birken, P. and Gassner, G. J. and Klöfkor, R.: An finite volume based multigrid preconditioner for DG-SEM for convection-diffusion. WCCM-ECCOMAS2020 (2021). <https://doi.org/10.23967/wccm-eccomas.2020.21>
- [17] Birken, P., Dedner, A., Kasimir, J., Klöfkor, R.: A multigrid preconditioner for discontinuous galerkin methods applied to numerical weather prediction. In: ECCOMAS 2024 (2024). <https://doi.org/10.23967/eccomas.2024.027>
- [18] Birken, P.: Optimizing Runge-Kutta smoothers for unsteady flow problems. ETNA **39**, 298–312 (2012)
- [19] Blom, D.S., Birken, P., Bijl, H., Kessels, F., Meister, A., Zuijlen, A.H.: A comparison of rosenbrock and esdirk methods combined with iterative solvers for unsteady compressible flows. Adv. Comp. Math. **42**, 1401–1426 (2016) <https://doi.org/10.1007/s10444-016-9468-x>
- [20] Schuster, D., Brdar, S., Baldauf, M., Dedner, A., Klöfkor, R., Kröner, D.: On discontinuous Galerkin approach for atmospheric flow in the mesoscale with and without moisture. Meteorologische Zeitschrift **23**(4), 449–464 (2014) <https://doi.org/10.1127/0941-2948/2014/0565>
- [21] Dedner, A., Klöfkor, R.: Extendible and Efficient Python Framework for Solving Evolution Equations with Stabilized Discontinuous Galerkin Method. Commun. Appl. Math. Comput. **4**, 657–696 (2022) <https://doi.org/10.1007/s42967-021-00134-5>
- [22] Kopriva, D.A., Gassner, G.: On the Quadrature and Weak Form Choices in Collocation Type Discontinuous Galerkin Spectral Element Methods. J. Sci. Comput. **44**, 136–155 (2010) <https://doi.org/10.1007/s10915-010-9372-3>
- [23] Kopriva, D.A., Woodruff, S.L., Hussaini, M.Y.: Computation of electromagnetic scattering with a non-conforming discontinuous spectral element method. Int. J. Numer. Methods Eng. **53**(1), 105–122 (2002) <https://doi.org/10.1002/nme.394>
- [24] Toro, E.F.: Riemann Solvers and Numerical Methods for Fluid Dynamics. Springer, Berlin, Heidelberg (2009). <https://doi.org/10.1007/b79761>
- [25] Brdar, S., Dedner, A., Klöfkor, R.: Compact and stable Discontinuous Galerkin methods for convection-diffusion problems. SIAM J. Sci. Comput. **34**(1), 263–282 (2012) <https://doi.org/10.1137/100817528>
- [26] Dedner, A., Girke, S., Klöfkor, R., Malkmus, T.: The DUNE-FEM-DG module. ANS **5**(1) (2017) <https://doi.org/10.11588/ans.2017.1.28602>
- [27] Ellsiepen, P.: Zeit- und ortsadaptive Verfahren angewandt auf Mehrphasenprobleme poröser Medien. PhD thesis, University of Stuttgart (1999)

- [28] Knoll, D.A., Keyes, D.E.: Jacobian-free Newton-Krylov methods: a survey of approaches and applications. *J. Comput. Phys.* **193**(2), 357–397 (2004) <https://doi.org/10.1016/j.jcp.2003.08.010>
- [29] Eisenstat, S.C., Walker, H.F.: Choosing the Forcing Terms in an Inexact Newton Method. *SIAM J. Sci. Comput.* **17**(1), 16–32 (1996) <https://doi.org/10.1137/0917003>
- [30] Kasimir, J.: Subgrid finite volume preconditioner for Discontinuous Galerkin implemented in the DUNE framework. Master thesis, Lund University (2021). <https://lup.lub.lu.se/student-papers/search/publication/9065436>
- [31] Witherden, F.D., Vincent, P.E.: On Nodal Point Sets for Flux Reconstruction. *J. Comput. Appl. Math.* **381** (2021) <https://doi.org/10.1016/j.cam.2020.113014>
- [32] Birken, P., Linders, V.: Conservation properties of iterative methods for implicit discretizations of conservation laws. *J. Sci. Comput.* **92** (2021) <https://doi.org/10.1007/s10915-022-01923-7>
- [33] Linders, V., Birken, P.: Locally conservative and flux consistent iterative methods. *SIAM J. Sci. Comput.* (2023) <https://doi.org/10.1137/22M1503348>
- [34] Dedner, A.: Solving the system of Radiation Magnetohydrodynamics for solar physical simulations in 3d. PhD thesis, Universität Freiburg (2003). <https://doi.org/urn:nbn:de:bsz:25-opus-10989>
- [35] Ketcheson, D.I.: Highly Efficient Strong Stability-Preserving Runge-Kutta Methods with Low-Storage Implementations. *SIAM J. Sci. Comput.* **30**(4), 2113–2136 (2008) <https://doi.org/10.1137/07070485X>
- [36] Skamarock, W.C., Klemp, J.B.: Efficiency and Accuracy of the Klemp-Wilhelmson Time-Splitting Technique. *Monthly Weather Review* **122** (1994) [https://doi.org/10.1175/1520-0493\(1994\)122\(2623:EAAOTK\)2.0.CO;2](https://doi.org/10.1175/1520-0493(1994)122(2623:EAAOTK)2.0.CO;2)
- [37] Robert, A.: Bubble Convection Experiments with a Semi-Implicit Formulation of the Euler Equations. *J. Atmos. Sci.* **50** (1993) [https://doi.org/10.1175/1520-0469\(1993\)050\(1865:BCEWAS\)2.0.CO;2](https://doi.org/10.1175/1520-0469(1993)050(1865:BCEWAS)2.0.CO;2)
- [38] Brdar, S., Baldauf, M., Dedner, A., Klöforn, R.: Comparison of dynamical cores for NWP models: comparison of COSMO and DUNE. *Theor. Comput. Fluid Dyn.* **27**(3-4), 453–472 (2013) <https://doi.org/10.1007/s00162-012-0264-z>
- [39] Straka, J.M., Wilhelmson, R.B., Wicker, L.J., Anderson, J.R., Droegemeier, K.K.: Numerical solutions of a non-linear density current: A benchmark solution and comparisons. *Int. J. Num. Meth. Fluids* **17**, 1–22 (1993) <https://doi.org/10.1002/fld.1650170103>

- [40] Dedner, A., Klöforn, R., Nolte, M., Ohlberger, M.: A Generic Interface for Parallel and Adaptive Scientific Computing: abstraction Principles and the DUNE-FEM Module. *Computing* **90**(3–4), 165–196 (2010) <https://doi.org/10.1007/s00607-010-0110-3>

A Modified Newton-Cotes formula for finite volume cell centers

A quadrature exact for polynomials of degree $k = 3$ with quadrature points corresponding to the cell centers of the finite volume grid from Figure 1 is given by the following quadrature points G_i and weights ω_i for $i = 0, 1, 2, 3$ in one dimension

$$\begin{aligned} G_0 &= \frac{1}{8}, \quad \omega_0 = \frac{1625}{6000} & G_1 &= \frac{3}{8}, \quad \omega_1 = \frac{1375}{6000} \\ G_2 &= \frac{5}{8}, \quad \omega_2 = \frac{1375}{6000} & G_3 &= \frac{7}{8}, \quad \omega_3 = \frac{1625}{6000} \end{aligned}$$

Appropriate quadratures for higher dimensions are formed through tensor product of the 1d quadrature. Weights for other polynomial degrees can be found in the class `ModifiedNewtonCotes` in the DUNE-FEM library [40].